Substrate-Integrated Waveguides in Glass Interposers with Through-Package-Vias

Jialing Tong, Venky Sundaram, Aric Shorey[+], and Rao Tummala
3D Systems Packaging Research Center
Georgia Institute of Technology, Atlanta, GA, USA
[+]Corning Incorporated, Corning, NY, USA
jtong@gatech.edu

Abstract

This paper presents, for the first time, substrate-integrated waveguides (SIWs) in ultra-thin glass with through-package-vias (TPVs). An SIW operating at 20 GHz was designed in bare glass substrates to support the dominant TE_{10} mode and to avoid exciting TE_{20} mode. The simulated propagation constant confirmed the proper design for one-mode excitation, while the distributions of electromagnetic fields and surface current were examined and they exhibited similar patterns to those in dielectric-filled rectangular waveguides. Furthermore, the simulated S-parameter shows that the insertion loss at 20 GHz is 0.67 dB/cm, and 100% relative bandwidth was achieved. Finally, the impacts of TPV taper and the variability of the glass thickness and TPV pitch on the electrical performance of the SIW in glass interposers with TPVs were studied and presented.

I. Introduction

Substrate-integrated waveguides (SIWs) were first proposed to integrate planar and non-planar circuits in mm-wave systems [1]. In these studies, SIWs were optimized for ultra-high speed digital interconnections [2], passive devices such as circulators [3], couplers [4, 5], filters [6, 7], and antennas [8, 9]. Most of the published research advances in SIWs were based on organic substrates, due to their wide-spread availability and usability with low-dielectric loss and mature printed circuit board (PCB) fabrication processes.

In contrast to organic substrates, glass substrates have several advantages over organic substrates as well as over silicon interposers due to the intrinsic characteristics of low electrical loss, tailorable coefficient of thermal expansion (CTE), high-build dimensional stability, smooth surface, and scalability to ultra-thin and large panel size manufacturing for low-cost [10]. Glass substrates have already been demonstrated for RF and microwave applications, including inductors for RF front-end modules operating in the GSM band [11]. Glass substrates have been characterized at mm-wave frequencies showing stable dielectric constant and low-loss at mm-wave bands even in the presence of moisture [12].

There are four compelling reasons why glass is an ideal candidate for mm-wave modules: 1) glass has excellent dimensional stability, much better than organic substrates, beneficial for high-precision circuit definition; glass has much lower dielectric loss than silicon and most organics; 2) glass has ultra-smooth surfaces for lowest interface losses; 3) glass is scalable to large panel size manufacturing leading to low-cost per module; and 4) glass has the CTE that is closely matched to RF ICs for high interconnection reliability. For all these reasons, glass is a compelling platform for mm-wave and RF systems.

In this paper, an SIW operating at 20 GHz was designed in bare glass substrates with TPVs and two-metal re-distribution layers (RDL). To excite the dominant TE_{10} mode and to avoid exciting TE_{20} mode, previously reported design equations [13] were used at first to determine the waveguide width. A detailed 3D model of the designed SIW was then constructed using commercial 3D electromagnetic (EM) software to verify the design. In the current design, 130μm thin glass [14] was used as the core substrate, and a row of 60μm diameter TPVs at 120μm center-to-center pitch were placed at each lateral edge of the SIW to realize perfect electric conductor (PEC) boundary conditions. The fabrication procedure, for the designed SIW, started with TPV formation, followed by Ti-Cu sputtering to achieve good adhesion to the smooth glass surfaces and copper was then plated to the target thickness using a double-side semi-additive process (SAP). All the fabrication processes are scalable to large panel sizes, to realize SIWs and mm-wave modules at much lower cost and higher performance than silicon interposers. The simulated electromagnetic fields and the surface currents had a similar distribution pattern to those in typical dielectric-filled rectangular waveguides. The simulated results indicated that the SIW had 0.67 dB/cm insertion loss at 20 GHz and 100% relative bandwidth. Finally, the effects of TPV taper angle and the variability of the glass thickness and TPV pitch, due to the fabrication process variations, were modeled and are presented here.

In Section II, a detailed design of SIW in glass is described. Then, the electromagnetic properties of the designed SIW are presented in Section III. Finally, the analysis and discussion of the TPV taper and its variability are presented in Section IV. Section V summarizes and concludes these studies.

II. Design of Glass Substrate-Integrated Waveguides

Glass, as a dielectric material, was used for SIWs here, and thus, its electrical properties had to be known to proceed with the design. Based on the design equations given in prior art and the specification of 20 GHz operation, the critical dimensions of one SIW were determined for unique propagation mode. Finally, the propagation constant was examined to ensure the dominant TE_{10} mode. In this section, the design of the SIW for TE_{10} propagation will be elaborated

Dimensional Design

For this study, alkali-free boroaluminosilicate glass (SGW3 from Corning) was used and the initial electrical properties were extracted from vendor provided data. The

permittivity and the loss tangent of SGW3 are depicted in Fig. 1, from which the permittivity is estimated to be 5.05 and the loss tangent is estimated to be 0.0068 at 20 GHz, proving the superior electrical performance of glass substrates up to 20 GHz.

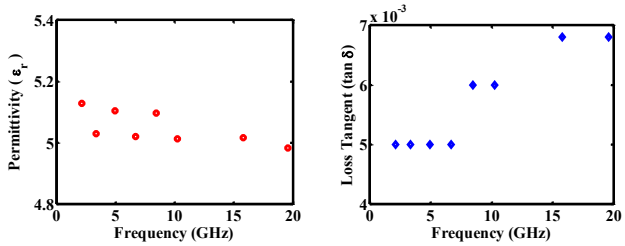

Fig. 1. (a) The permittivity, and (b) The loss tangent of Corning SGW3 glass characterized up to 20 GHz.

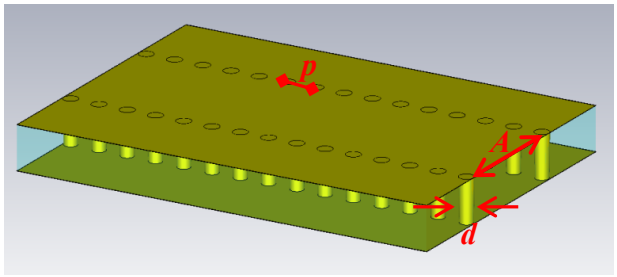

Fig. 2. Physical structure of SIW: p is the center-to-center pitch of adjacent TPVs; A is the center-to-center width between two rows of TPVs; d is the TPV diameter.

Based on the physical structure of Fig. 2, the critical dimensions to be designed in 130μm thin glass included the diameter of TPVs denoted by d, the center-to-center pitch of adjacent TPVs denoted by p, and the center-to-center width between two rows of TPVs denoted by A. The diameter of TPVs was set to be d = 60μm, which is well below the upper limit [13] and is convenient for metallization by sputtering, while the center-to-center pitch of adjacent TPVs was designed to be $p = 2 \cdot d$ = 120μm to minimize the radiation loss. The last design parameter is the center-to-center width between two rows of TPVs, also known as the width of the SIW, which is literally the most important parameter. On one hand, the width of the SIW has to be carefully designed so that at 20 GHz, TE_{10} mode will be the only propagation mode while the second higher order TE_{20} mode will be suppressed. On the other hand, because the phase around 20 GHz should be as linear as possible, the cutoff frequency of TE_{10} mode - f_c is designed at 15 GHz. Using the following two design equations [13], the width of the SIW could be calculated

$$A^* = \frac{C_0}{2 f_c \sqrt{\varepsilon_r}} \tag{1}$$

$$A = \frac{1}{2}\left[A^* + \sqrt{\left(A^* + 0.54d\right)^2 - 0.4d^2} \right] + 0.27d \tag{2}$$

where C_0 is the speed of light in vacuum, f_c is the designed cutoff frequency of TE_{10} mode, i.e. 15 GHz, and ε_r is the relative permittivity of the glass.

Propagation Constant and Wave Impedance

A detailed 3D model was constructed using Computer Simulation Technology (CST) 3D EM software to initially verify the design computed in the previous section. Initially, the attenuation constant α was examined. Theoretically, the attenuation constant is expected to be close to zero when the mode is excited, but it should be a non-zero value when the mode is not excited. As shown in Fig. 3, from 10 GHz to the first cutoff frequency for TE_{10} mode, no electromagnetic field is excited, rendering α to be non-zero; afterward, the expected first TE_{10} mode starts to propagate till the second TE_{20} mode starts at the cutoff frequency for TE_{20} mode. At 20 GHz, it is obvious that only TE_{10} is generated, which satisfies one-mode propagation requirement.

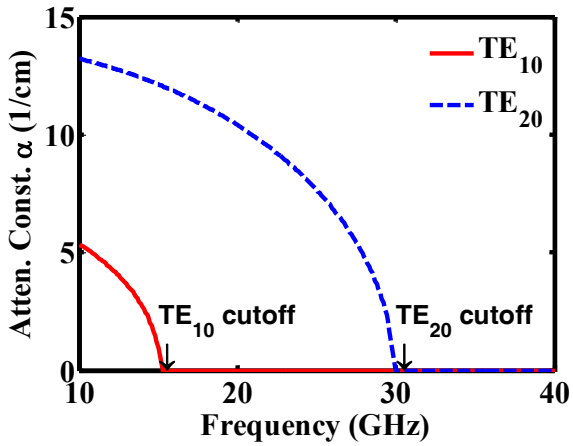

Fig. 3. The attenuation constants (α) of TE_{10} and TE_{20} modes as a function of frequency.

Another requirement is the phase linearity around 20 GHz which was evaluated again in CST through the phase constant β. The simulated phase constants are plotted in Fig. 4, from which it can be seen that TE_{10} mode is confirmed to be the only propagation mode and the phase around 20 GHz is essentially linear as required. Thus far, it is guaranteed by the simulation that TE_{10} mode is the dominant mode in the designed SIW and the phase around 20 GHz is linear.

Finally, the wave impedance was investigated to ensure the reflection to be low. The wave impedances are plotted against frequency in Fig. 5, and they vary drastically below the cutoff frequencies. However, once the frequency goes beyond the cutoff frequencies, they remain approximately the same. Therefore, the wave impedance of TE_{10} mode is unchanged around 20 GHz.

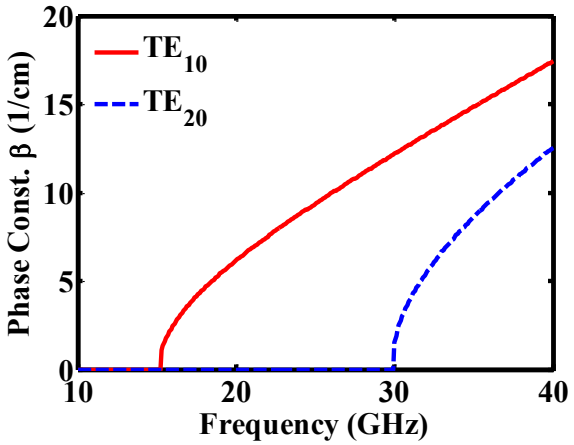

Fig. 4. The phase constants (β) of TE_{10} and TE_{20} modes as a function of frequency.

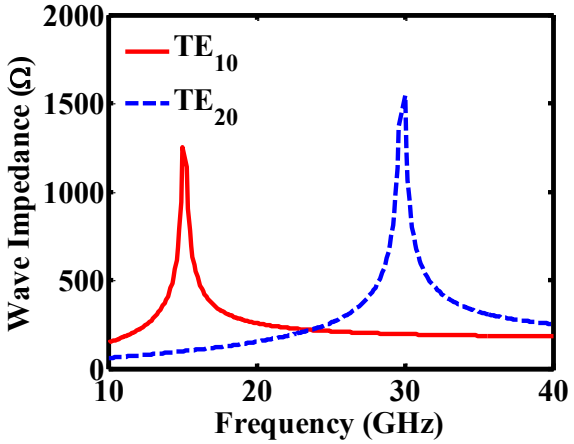

Fig. 5. The wave impedances of TE_{10} and TE_{20} modes as a function of frequency.

III. Electromagnetic Properties

In the SIW, since the signal is propagating in terms of electric and magnetic fields, it is of great importance to investigate its electromagnetic properties. Basically, the S-parameters, namely S_{11} and S_{21}, the patterns of the electric and magnetic field, and the surface currents are detailed in this section.

S-Parameters

The magnitude of S_{11} and S_{21} is depicted in Fig. 6; the 3dB cutoff frequency for TE_{10} is 15.22 GHz that is close to the tentative 15 GHz, and consequently the 3dB cutoff frequency for TE_{20} is $2\times15.22=30.44$ GHz. The return loss is more than 20 dB within the range of 15.22 GHz to 30.44 GHz while the insertion loss is about 0.67 dB/cm, showing the superior performance of the glass as the core of SIW. Beyond 30.44 GHz, even though the simulated results remain nearly unchanged, S_{21} will deviate from the value shown in Fig. 6 due to the generation of TE_{20} mode.

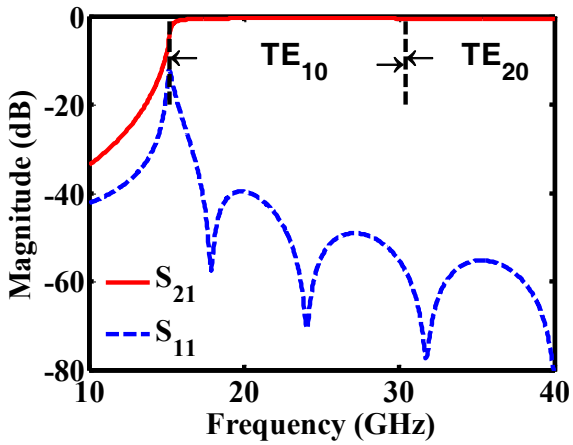

Fig. 6. The magnitude of the simulated S_{21} and S_{11} in dB as a function of frequency.

In addition to the magnitude, the phase of S_{21} was investigated and is depicted in Fig. 7. Similar to the results given in Fig. 4, the phase around 20 GHz is linear. Now, it can be concluded that the designed SIW has 100% bandwidth ((30.44-15.22)/15.22 %) and 0.67 dB/cm loss at 20 GHz with linear phase.

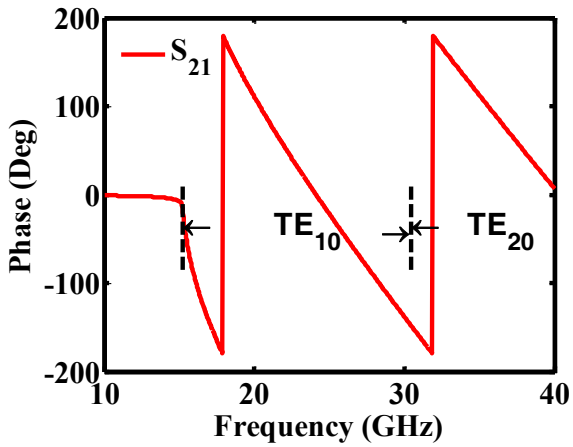

Fig. 7. The phase of the simulated S_{21} in Degrees as a function of frequency.

Electromagnetic Fields and Surface Currents

The simulated patterns of the electric field, the magnetic field and the surface currents are given in Fig. 8, Fig. 9 and Fig. 10, respectively. In Fig. 8 (a), the electric field is vertically oriented and is travelling along the SIW; in Fig. 8 (b), the strength of the electric field over the cross section has half-sine-wave distribution. In Fig. 9 (a), the magnetic field is horizontally oriented and is circulating inside the SIW; in Fig. 8 (b), the magnetic field starts outward at left and goes inward at right, and the strength over the cross section also has half-sine-wave distribution. In Fig. 10, the magnitude of the surface currents is provided in the perspective view. Since the

substrate thickness is relatively thin (130 μm), the conductor loss due to the current flowing through TPVs can be neglected. In other words, the conductor loss mainly comes from the top and bottom metal planes. Overall, the distributions of the fields, including the electric field, the magnetic field and the surface currents, are almost the same with those in typical dielectric-filled rectangular waveguides.

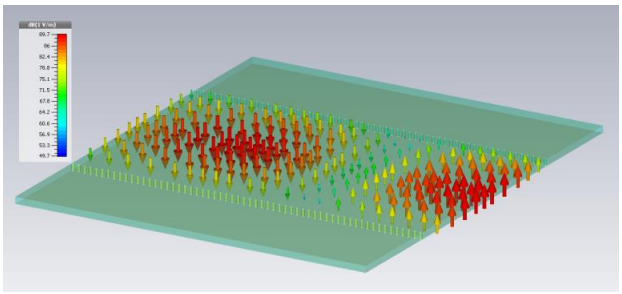

(a)

(b)

Fig. 8. (a) The perspective view, and (b) The cross-section view of the simulated electric field distribution of TE_{10} mode at 20 GHz.

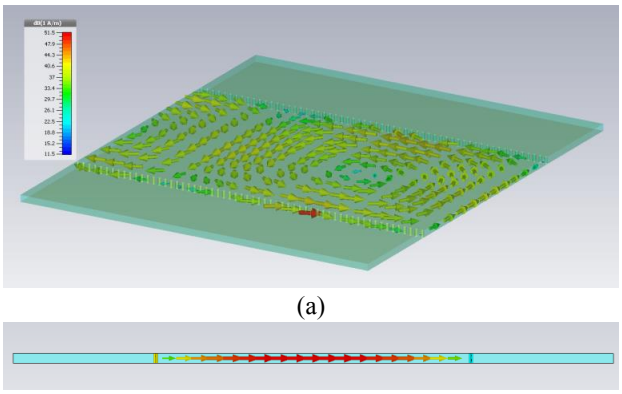

(a)

(b)

Fig. 9. (a) The perspective view, and (b) The cross-section view of the simulated magnetic field distribution of TE_{10} mode at 20 GHz.

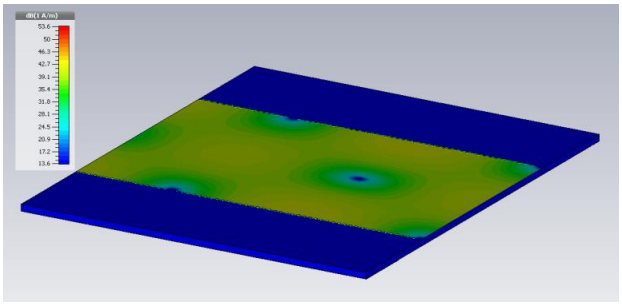

Fig. 10. The perspective view of the magnitude of the simulated surface current of TE_{10} mode at 20 GHz.

IV. Analysis of Glass Substrate-Integrated Waveguide

TPVs in glass have taper shape, and the fabrication process introduces the variability of the glass thickness and TPV pitch. In this section, detailed analysis of the effect of tapered TPVs on the insertion loss is studied first. Then, the effect of the variability of the glass thickness and the TPV pitch on the insertion loss and the wave impedance is investigated.

Effect of TPV Taper

Fig. 11 (a) shows the tapered profile and Fig. 11 (b) shows the circular opening of TPVs from Corning. This taper is what is given by current processes and herein the effects of the TPV profile on performance will be studied.

(a) (b)

Fig. 11. The (a) cross-section view and (b) the top view of TPVs in Corning SGW3 glass.

To quantitatively gauge the taper effect on the mm-wave performance, the insertion loss was chosen as the criterion. Based on the previously-designed SIW, both rows of TPVs were modelled as conical shape. The schematic view of these TPVs is depicted in Fig. 12 (a), where the top diameter is fixed at 60μm, but the taper angle denoted by θ varies. Three scenarios were simulated by CST: 1) in 100μm glass, the taper angle varied from 75° to 89°; 2) in 300μm glass, the taper angle varied from 86° to 88°; 3) in 500μm glass, the taper angle varied from 87° to 88°. The bottom diameters in these three scenarios are plotted in Fig. 12 (b).

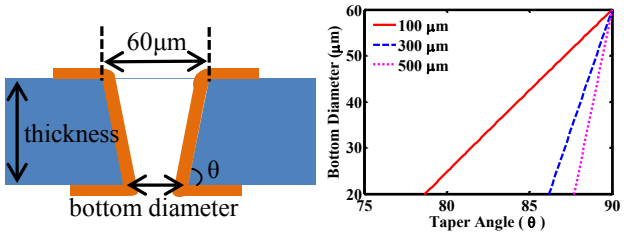

(a) (b)

Fig. 12. (a) The schematic view of tapered TPV with the taper angle denoted as θ; (b) The change of the bottom diameter as the taper angle varies.

Since the operation frequency was specified to be 20 GHz, the insertion loss at this frequency point was evaluated for various taper angles in three cases of different glass thicknesses, i.e. 100μm, 300μm and 500μm. The insertion loss

at 20 GHz was retrieved from the simulated results and is presented in Fig. 13. There are two conclusions that can be derived in this figure. Using thinner glass for SIWs results in larger insertion loss at 20 GHz. The impact of glass thickness on the loss will be discussed in detail in the following sub-section. More importantly, for each glass thickness, when the taper angle or the bottom diameter varies, the insertion loss at 20 GHz remains relatively unchanged. This is because compared to the guide wavelength the substrate thickness and the TPV diameter are electrically small, making the taper effect of TPVs almost negligible.

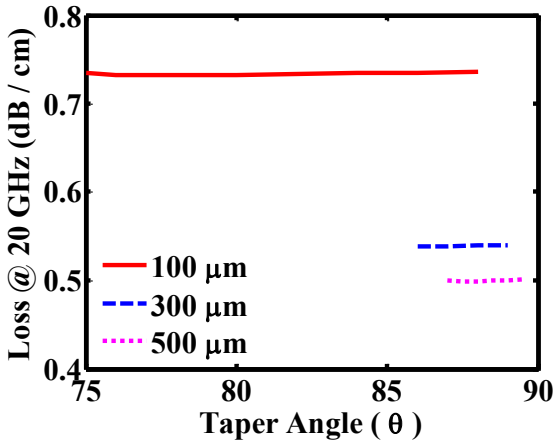

Fig. 13. The insertion loss at 20 GHz for various taper angles in three different glass thicknesses: 100μm, 300μm and 500μm.

Effect of Variability

In addition to the taper shape of TPVs, the glass thickness and the pitch of TPVs may deviate from the pre-defined values. As a result, the electrical performance of SIWs might be degenerated.

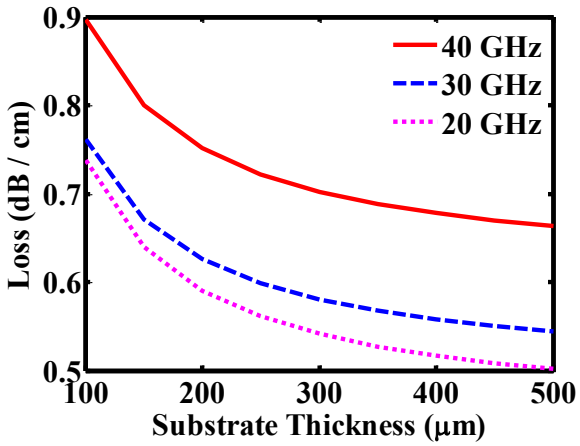

Fig. 14. The insertion loss at 40, 30, and 20 GHz for various glass substrate thicknesses with the straight TPVs.

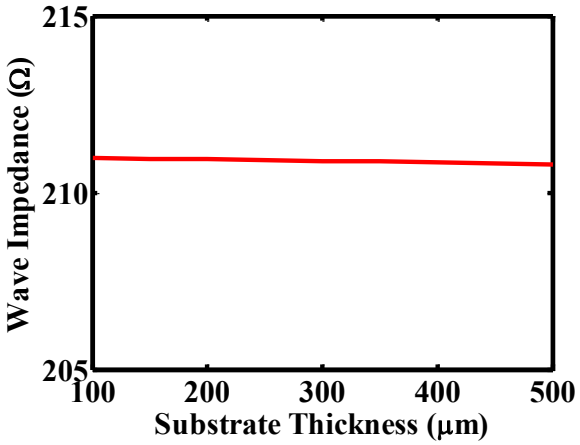

Fig. 15. The wave impedance as a function of substrate thicknesses.

The variability of the glass thickness has two potential impacts: the insertion loss and the wave impedance. Similar to what was presented for the taper effect, the insertion losses at 40, 30, and 20 GHz were used as the criteria. According to the simulated results shown in Fig. 14, it was found that the losses at the three frequency points all decreased as the substrate thickness increased. Recalling the electric field derived in [15], the vertical component of the electric field was inversely proportional to the substrate thickness. Thus, when the substrate thickness increases, the strength of the electric field decreases and the dissipated energy through the movement of charges under the decreased electric field decreases consequently, resulting in reduced loss. As the wave impedance is directly related to the reflection, the effect of the variability of the glass thickness on the wave impedance is equally important for study. From the computational results by CST, the wave impedance is depicted in Fig. 15. Herein, it is found that the wave impedance is nearly not influenced by the substrate thickness, which matches to the equation in [15].

Lastly, the effect of variability in TPV pitch on the electrical performance was studied. Deviations in TPV pitch had a marginal effect on the insertion loss, as observed from the graph of the Fig. 16. Insertion losses indeed varied by less than 1% from the nominal 0.67 dB/cm obtained for the designed 120μm pitch, when TPV pitch was varied in the 100-480μm ranges. This can be attributed to the relatively small TPV diameter and thickness of the substrate core, resulting in minimum radiation loss. Taper TPVs have more loss than straight TPVs, especially when the pitch increases to more than 5 times of the TPV diameter, as it is shown in Fig. 16. However, the difference is still not significant, and at pitch less than three times of the TPV diameter the difference is ignorable, which is in consistent with the results shown in Fig. 13.

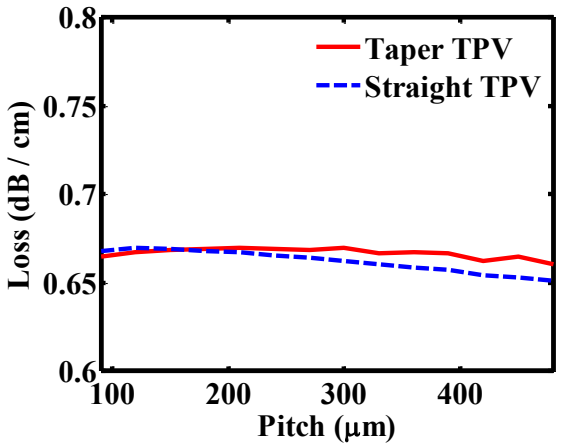

Fig. 16. The insertion loss at 20 GHz as a function of TPV pitch.

V. Conclusions

This paper presented, for the first time, the modeling and design of SIWs in thin glass substrates with TPVs, exhibiting ultra-low signal loss and ultra-wide bandwidth. The SIWs were designed at 20 GHz with unique TE_{10} mode propagation, and the simulated propagation constant showed that $TE_{20,}$ the second higher order mode, was effectively suppressed. The patterns of the electromagnetic fields and the surface currents were investigated, similar to those in dielectric-filled rectangular waveguides. Based on the S-parameters computed by 3D EM software, the relative bandwidth was determined to be 100% and the insertion loss at 20 GHz was 0.67 dB/cm. Finally, the effects of TPV taper, the variability of the glass thickness and TPV pitch were studied. It was shown that TPV taper and pitch have very little impact on the insertion loss, due to the small TPV diameter and thinness of glass substrate. Thicker glasses resulted in lower loss because of the reduced field strength. These results indicate that glass is an ideal package substrate for millimeter-wave systems.

Acknowledgments

The authors would like to thank the full-member and supply-chain companies of the Low-cost Glass Interposer and Package (LGIP) consortium at the 3D Systems Packaging Research Center (PRC), Georgia Institute of Technology, Atlanta.

References

1. K. Wu et al., "The substrate integrated circuits - a new concept for high-frequency electronics and optoelectronics," in *Proceeding of 2003 TELSIKS*, vol.1, pp. 2-9, 1-3 Oct. 2003.
2. J. J. Simpson et al., "Substrate integrated waveguides optimized for ultrahigh-speed digital interconnects," *IEEE Transactions on MTT*, vol.54, no.5, pp.1983-1990, May 2006.
3. W. D'Orazio et al., "Substrate-Integrated-Waveguide Circulators Suitable for Millimeter-Wave Integration," *IEEE Transactions on MTT*, vol.54, no.10, pp.3675-3680, Oct. 2006.
4. B. Liu et al., "Half Mode Substrate Integrated Waveguide 180° 3-dB Directional Couplers," *IEEE Transactions on MTT*, vol.55, no.12, pp.2586-2592, Dec. 2007.
5. T. Djerafi et al., "Ring-Shaped Substrate Integrated Waveguide Wilkinson Power Dividers/Combiners," *IEEE Transactions on CPMT*, vol.4, no.9, pp.1461-1469, Sept. 2014.
6. X.-P. Chen et al., "Substrate Integrated Waveguide Cross-Coupled Filter With Negative Coupling Structure," *IEEE Transactions on MTT*, vol.56, no.1, pp.142-149, Jan. 2008.
7. X.-P. Chen et al., "Substrate Integrated Waveguide Filter With Improved Stopband Performance for Satellite Ground Terminal," *IEEE Transactions on MTT*, vol.57, no.3, pp.674-683, March 2009.
8. M. Henry et al., "Millimeter Wave Substrate Integrated Waveguide Antennas: Design and Fabrication Analysis," *IEEE Transactions on AP*, vol.32, no.1, pp.93-100, Feb. 2009.
9. Y. Cai et al., "Bandwidth Enhancement of SIW Horn Antenna Loaded With Air-Via Perforated Dielectric Slab," *IEEE AWPL*, vol.13, pp.571-574, 2014.
10. V. Sukumaran et al., "Low-Cost Thin Glass Interposers as a Superior Alternative to Silicon and Organic Interposers for Packaging of 3-D ICs," *IEEE Transactions on CPMT*, vol.2, no.9, pp.1426-1433, Sept. 2012
11. J.-M. Yook et al, "High Performance IPDs (Integrated Passive Devices) and TGV (Through Glass Via) Interposer Technology using the Photosensitive Glass," in *Proceeding of 2011 IEEE 61st ECTC*, pp. 255-261, May 31-June 3 2011.
12. J. Leib et al., "Low temperature glass-thin-films for use in power applications," in *Proceeding of 2014 IEEE 64th ECTC*, pp. 41-46, May 27-30 2014.
13. J.E. Rayas-Sanchez et al., "A general EM-based design procedure for single-layer substrate integrated waveguide interconnects with microstrip transitions," in *Proceeding of 2008 IEEE MTT-S*, pp.983-986, 15-20 June 2008.
14. Corning Incorporated, "Corning® Semiconductor Glass Wafer Product Information Sheet," http://www.corning.com/WorkArea/showcontent.aspx?id=49853
15. D. M. Pozar, Microwave Engineering (4th Edition), Wiley Global Education, 2011, pp. 96–121.